2022

Using Local Entropy Generation Rate in Air-Side Heat Exchanger Design

Max Friestad

Anthony M. Jacobi

Using Local Entropy Generation Rate in Air-Side Heat Exchanger Design

Max Friestad[1]*, Anthony Jacobi[2]

[1]The University of Illinois at Urbana-Champaign, Department of Mechanical Science and Engineering, Urbana, IL, USA
friesta2@illinois.edu

[2]The University of Illinois at Urbana-Champaign, Department of Mechanical Science and Engineering, Urbana, IL, USA
a-jacobi@illinois.edu

* Corresponding Author

ABSTRACT

The use of computational fluid mechanics (CFD) in air-side heat exchanger design is widespread and routine in the HVAC&R industry. In some cases, CFD is used to develop reduced-order models, which in turn become part of a larger, systematic optimization. While truly revolutionary design, say through topology optimization and machine learning, may be within grasp, widespread engineering adoption appears to be years or more away. However, an intermediate step based on developing a deeper understanding of the physics is certainly within grasp. Namely, a numerical, local, Second-Law analysis of heat exchanger performance. In this paper, we make a compelling case for why this approach will provide new and better-informed design directions, and how it can be deployed without heroic means using any of the current CFD platforms. Furthermore, we explain how local entropy generation rates can be interpreted to better understand the ramifications of design on heat exchanger performance. With a louvered-fin heat exchanger example, we show that a Second-Law analysis of air-side performance will provide new insights into design, insights unavailable in a First-Law framework.

1. INTRODUCTION

Energy prices are now and will continue to be the primary determining factors of the total cost of everything we enjoy in modern society. HVAC&R devices that transform this energy are no different. A typical optimization statement for these devices is to *minimize* the total cost of the device for a *given* duty. For example, removing a given amount of heat from the condensing coils of a heat exchanger for as little electricity as possible. This strategy is based on the bedrock of the First Law of Thermodynamics which seeks to optimize based on energy into and out of the given system. The Second Law of Thermodynamics applied to CFD seeks to optimize based on the irreversibility *within* the system and is the subject of this paper.

A common argument against the Second-Law approach is that the First is much easier to understand and interpret. Another is that if a well-defined global optimum is found with the First, then the Second is unnecessary. Therefore, the Second Law is weak and should be avoided. This thought process works well for optimization but misses the usefulness of the Second Law. If one recognizes that the thermodynamic objective is indeed to move heat while doing the least work and that the Second Law identifies precisely when and where work is "wasted" (i.e., destroyed without serving the objective), then the Second Law is clearly valuable. The new objective can therefore be to minimize wasted work, and we do that by minimizing the rate of entropy generation. Wasted work and entropy generation are directly related through the Gouy-Stodola theorem (Gouy, 1889; Stodola, 1927):

$$\dot{W}_{destroyed} = T_0 \dot{S}_{gen} \tag{1}$$

In Eq. (1), T_o is the 'dead state' temperature. In air-conditioning systems that is the temperature to which the machine rejects heat, typically the outdoor temperature. Thus, the dead state might change with the weather; moreover, in some systems, it might be a different temperature, e.g., the temperature of deep space. The ambiguity of T_o is of no concern. It would suffice to state that "wasted work is proportional to the rate of entropy generation" as justification for entropy generation minimization. All that is needed to search for wasted work in an air-side flow is a way to calculate the rate of entropy generation. Then one can use that knowledge to understand what mechanism generates entropy and to seek an optimal heat exchanger design.

Following Bejan (1982), an entropy balance on a two-dimensional differential control volume yields the following volumetric rate of entropy generation:

$$\dot{S}'''_{gen} = \frac{1}{T}\left(\frac{\partial q_x}{\partial x} + \frac{\partial q_y}{\partial y}\right) - \frac{1}{T^2}\left(q_x \frac{\partial T}{\partial x} + q_y \frac{\partial T}{\partial y}\right) + \rho\left(\frac{\partial s}{\partial t} + v_x \frac{\partial s}{\partial x} + v_y \frac{\partial s}{\partial y}\right) \tag{2}$$

In this equation, the first two terms represent entropy transfer due to conductive heat transfer, and the final term represents the net entropy convection out of the control volume. Making this expression three-dimensional and using Gibbs notation,

$$\dot{S}'''_{gen} = \frac{1}{T}\left(\nabla \bullet \vec{q}\right) - \frac{1}{T^2}\left(\vec{q} \bullet \nabla T\right) + \rho \frac{Ds}{Dt} \tag{3}$$

The first law applied to such a control volume gives the following:

$$\rho \frac{Du}{Dt} = -P\left(\nabla \bullet \vec{v}\right) - \left(\nabla \bullet \vec{q}\right) + \mu\Phi \tag{4}$$

Note that internal energy, u, appears on the left-hand side because pressure work is separately included as the first term on the right-hand side of the equation. The second term in the right-hand side of the equation is due to conductive heat transfer, and the final term is the "viscous dissipation function," which accounts for flow work conversion into thermal energy by viscous effects. You may recall that for a laminar, incompressible, Newtonian flow, the viscous dissipation function is

$$\Phi = 2\left[\left(\frac{\partial \mathrm{v_x}}{\partial \mathrm{x}}\right)^2 + \left(\frac{\partial \mathrm{v_y}}{\partial \mathrm{y}}\right)^2 + \left(\frac{\partial \mathrm{v_z}}{\partial \mathrm{z}}\right)^2\right] + \left(\frac{\partial \mathrm{v_x}}{\partial \mathrm{y}} + \frac{\partial \mathrm{v_y}}{\partial \mathrm{x}}\right)^2 + \left(\frac{\partial \mathrm{v_y}}{\partial \mathrm{z}} + \frac{\partial \mathrm{v_z}}{\partial \mathrm{y}}\right)^2 + \left(\frac{\partial \mathrm{v_z}}{\partial \mathrm{x}} + \frac{\partial \mathrm{v_x}}{\partial \mathrm{z}}\right)^2 \tag{5}$$

Writing du=Tds-Pdv in terms of density and using the substantial derivative gives:

$$\rho \frac{Ds}{Dt} = \frac{\rho}{T}\frac{Du}{Dt} - \frac{P}{\rho T}\frac{D\rho}{Dt} \tag{6}$$

Now solve Eq. (3) for ρDs/Dt, then substitute ρDs/Dt from Eq. (6). Substitute ρDu/Dt from Eq. (4) and note that for an incompressible flow, Dρ/Dt =0, as does the divergence of the velocity. Rearrange to solve for volumetric rate of entropy generation and you obtain:

$$\dot{S}'''_{gen} = -\frac{1}{T^2}\left(\vec{q} \bullet \nabla T\right) + \frac{\mu}{T}\Phi \tag{7}$$

Assuming isotropic, Fourier-Biot conduction in the fluid

$$\vec{q} = -k\nabla T \tag{8}$$

Using Eq. (8) in (7) gives the final expression we seek:

$$\dot{S}'''_{gen} = \dot{S}'''_{gen,T} + \dot{S}'''_{gen,V} \tag{9a}$$

where

$$\dot{S}'''_{gen,T} = \frac{k}{T^2}\left(\nabla T \bullet \nabla T\right) \tag{9b}$$

and

$$\dot{S}'''_{gen,V} = \frac{\mu}{T}\Phi \tag{9c}$$

Arranging Eq. (9a) as shown, emphasizes that local entropy generation for an air-side flow has two distinct and different mechanisms: entropy generation due to heat flow over finite temperature differences, and entropy generation due to the irreversible conversion of work to heat by viscosity. The two contributions in their two-dimensional form, realizing the three-dimensional form is a trivial extension and hold no surprises (cf. Eq 5):

$$\dot{S}'''_{gen,T} = \frac{k}{T^2}\left[\left(\frac{\partial T}{\partial x}\right)^2 + \left(\frac{\partial T}{\partial y}\right)^2\right] \tag{10a}$$

$$\dot{S}'''_{gen,V} = \frac{\mu}{T}\left\{2\left[\left(\frac{\partial v_x}{\partial x}\right)^2 + \left(\frac{\partial v_y}{\partial y}\right)^2\right] + \left(\frac{\partial v_x}{\partial y} + \frac{\partial v_y}{\partial x}\right)^2\right\} \tag{10b}$$

Clearly, temperature gradients give rise to entropy generation, and separately, velocity gradients give rise to entropy generation. By integrating both contributions separately, it is possible to compare their relative magnitudes and thus decide where to focus design effort. Then the local variation provides information to where losses occur. This is best illustrated with an example of, in this case, a louvered fin heat exchanger.

2. METHODS

2.1 Design and Mesh

The louvered fin design that is discussed in this paper is shown in Figure 1. The design was chosen because it is one of the simplest forms of the louvered fin geometry used commonly in industrial applications. The design was drawn in ANSYS Design Modeler using the in-plane dimensions shown in Table 1 with reference to the standard nomenclature of Figure 2 from Park and Jacobi (2009). ANSYS Mechanical was then used to mesh the design using the built-in adaptive meshing and boundary inflation on the louver walls. The resulting unstructured grid was then repeatedly refined at the louver walls and solved until mesh independence of the solution was established. The mesh independence data is shown in Table 2 with mesh detail shown in Figure 3. Future changes in the design used the same meshing parameters as established here as a base case.

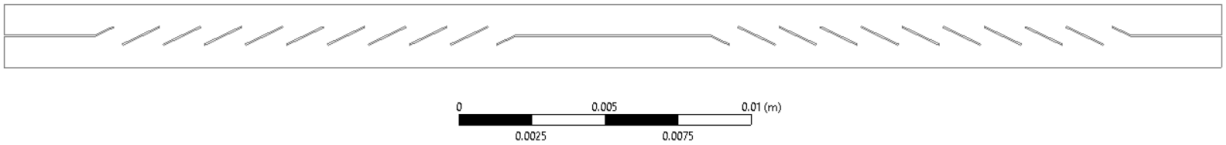

Figure 1: Louvered fin two-dimensional domain

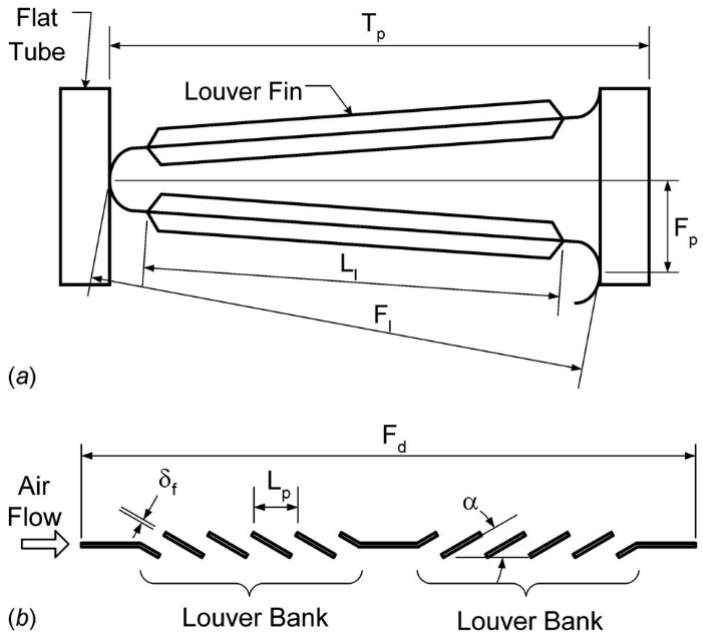

Figure 2: Louvered fin out-of-plane dimensions (a) and in-plane dimensions (b) (Park and Jacobi, 2009)

Table 1: Dimensions

In-plane				Out-of-plane			
δ_t [mm]	L_p [mm]	F_d [mm]	α [deg]	T_p [mm]	L_l [mm]	F_p [mm]	F_l [mm]
0.05	1.402	41.6	25.5	25	18.5	2.15	20

Table 2: Mesh independence

Wall Sizing [m]	Other Boundary Sizing [m]	Nodes	$\dot{S}_{gen,T}$ [W/K]	$\dot{S}_{gen,V}$ [W/K]	Change in $\dot{S}_{gen,T}$	Change in $\dot{S}_{gen,V}$
6.25×10^{-6}	5×10^{-5}	206633	0.1453	0.07902	-	-
3.125×10^{-6}	5×10^{-5}	393737	0.1377	0.07424	-5.2%	-6%

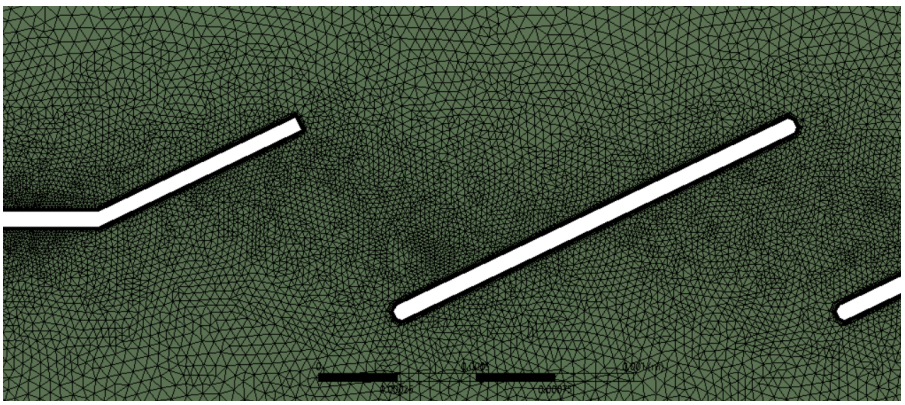

Figure 3: Mesh in detailed view

2.2 Code

ANSYS Fluent 19 was the code package chosen for the numerical solutions. Fluent uses the Finite Volume Method and has a wide range of modeling capabilities, among which include the $k-\epsilon$ Model and its derivatives. The Standard $k-\epsilon$ Model was the first developed by Launder and Spalding in 1974 for fully turbulent flows. Most heat exchangers with extended surfaces like louvered fins, however, have flows that relaminarize upon encountering these surfaces. The Standard version of this model is incapable of modeling the high shear stresses within the boundary layers, so wall functions are often used to force a pseudo-laminar boundary layer near the wall (Launder and Spalding, 1974). The newer Realizable $k-\epsilon$ Model modifies the eddy viscosity equation to perform better than the Standard Model for nearly every flow, including boundary layer flows with and without pressure gradients (Shih et al., 1995).

The steady Realizable $k-\epsilon$ Model of Eqs. 11-15 with standard wall functions was applied using the default parameters (ANSYS FLUENT 12.0 Theory Guide, 2009). The inlet condition on the left of Figure 1 was set to a velocity of 20.84 m/s which corresponds to a Reynolds number of 2000 based on louver pitch L_p, and the inlet turbulent intensity and viscosity ratio were 5% and 10, respectively. The outlet condition was set for ambient pressure and all louver surfaces were set for no-slip condition. The top and bottom of the domain were periodic boundaries which simulates infinite louvered surfaces placed in parallel.

$$\frac{\partial}{\partial x_j}(\rho k u_j) = \frac{\partial}{\partial x_j}\left[\left(\mu + \frac{\mu_t}{\sigma_k}\right)\frac{\partial k}{\partial x_j}\right] - \rho\overline{u_i' u_j'}\frac{\partial u_j}{\partial x_i} - \rho\epsilon \tag{11}$$

$$\frac{\partial}{\partial x_j}(\rho\epsilon u_j) = \frac{\partial}{\partial x_j}\left[\left(\mu + \frac{\mu_t}{\sigma_\epsilon}\right)\frac{\partial \epsilon}{\partial x_j}\right] + \rho C_1 S\epsilon - \rho C_2 \frac{\epsilon^2}{k + \sqrt{\nu\epsilon}} + S_\epsilon \tag{12}$$

$$C_1 = \max\left[0.43, \frac{\eta}{\eta + 5}\right] \tag{13}$$

$$\eta = S\frac{k}{\epsilon} \tag{14}$$

$$S = \sqrt{2S_{ij}S_{ij}} \tag{15}$$

The SIMPLE algorithm was chosen to reach a solution in which the values of x-velocity, y-velocity, and energy reached residuals of 10^{-6} or smaller, and continuity, k, and ϵ reached 10^{-3} or smaller. The spatial discretization for the turbulence parameters k, and ϵ were set to second order upwind schemes to match the other equations. Air was chosen as the fluid with the relevant properties shown in Table 3. The louver walls were given a constant temperature condition of 325 K with inlet condition of 300K.

Table 3: Properties of air

ρ [kg/m^3]	μ [kg/m-s]	C_p [J/kg-K]	k_{cond} [W/m-K]
1.225	1.7894 x 10^{-5}	1006.43	0.0242

3. RESULTS

Figure 4 shows the streamlines and log-scale contours of $\dot{S}'''_{gen,T}$, $\dot{S}'''_{gen,V}$, and $\dot{S}'''_{gen,Total}$. The results were compared with published correlations from Park and Jacobi 2009 using the Chilton and Colburn j-factor and Fanning f-factor. The relative difference of the solution j-factor and f-factor from the correlations were -4.0 % and -67 %, respectively. The total integrated entropy generations were 0.1453 W/K for $\dot{S}_{gen,T}$ and 0.07902 W/K for $\dot{S}_{gen,V}$, making the entropy generation due to temperature gradients about twice that of velocity gradients.

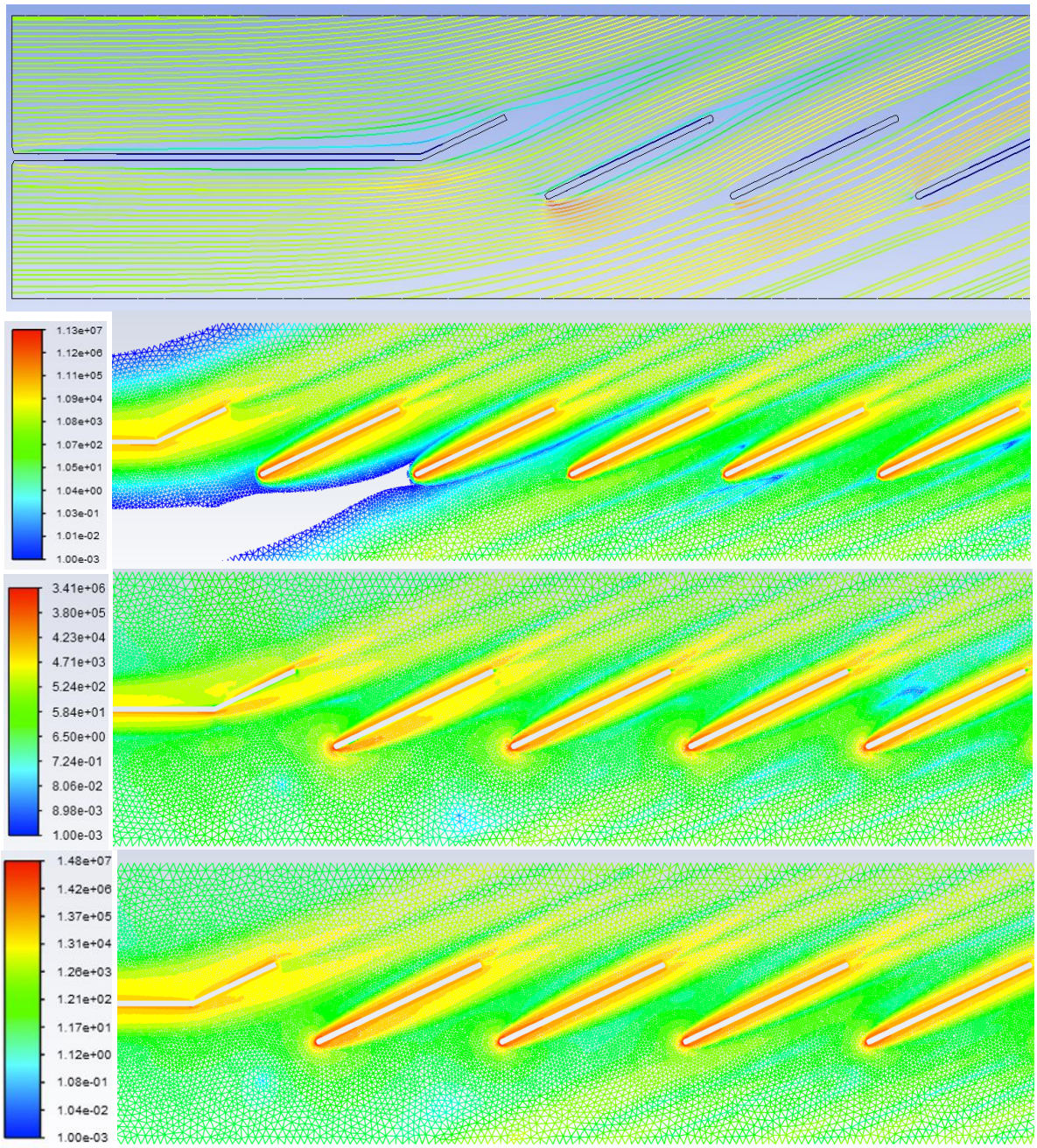

Figure 4: Invariable attack angle. Top to bottom: streamlines colored by velocity magnitude, log-scale contours of $\dot{S}'''_{gen,T}$, $\dot{S}'''_{gen,V}$, and $\dot{S}'''_{gen,Total}$

Figure 4 shows that most entropy generation occurs at the louver walls, as expected. A closer look at the first few fins reveals that there is significant entropy generation around the leading edge of each fin. Comparing $\dot{S}'''_{gen,V}$ with the streamlines one can see that the air experiences a sharp change in direction around the first few fins which causes separation of the boundary layer to the right of the leading edges along with large velocity gradients and therefore large $\dot{S}'''_{gen,V}$ in the stagnation region. The same is true downstream where the flow reverses direction before exiting the heat exchanger. One can also see that $\dot{S}'''_{gen,T}$ is concentrated near the fins at the leading edge as expected, and there are steeper temperature gradients on the upstream side of the fin as the higher flow velocity gradients convect heat away faster, especially in the first few fins of the turning flow.

The entropy generation in this design seems to arise from the abrupt change in direction that the fins force on the incoming air. One iteration of change in the base design may therefore be gradually changing the attack angle of the fins to slowly coax the air to flow evenly over the fins downstream. Figure 5 shows the new design in which the attack angle increases linearly up to the base case of 25.5 degrees then reverses in the same way downstream. The total integrated entropy generations were 0.1361 W/K for $\dot{S}_{gen,T}$ and 0.06039 W/K for $\dot{S}_{gen,V}$, a change of -6.3 % and -23.6 %, respectively.

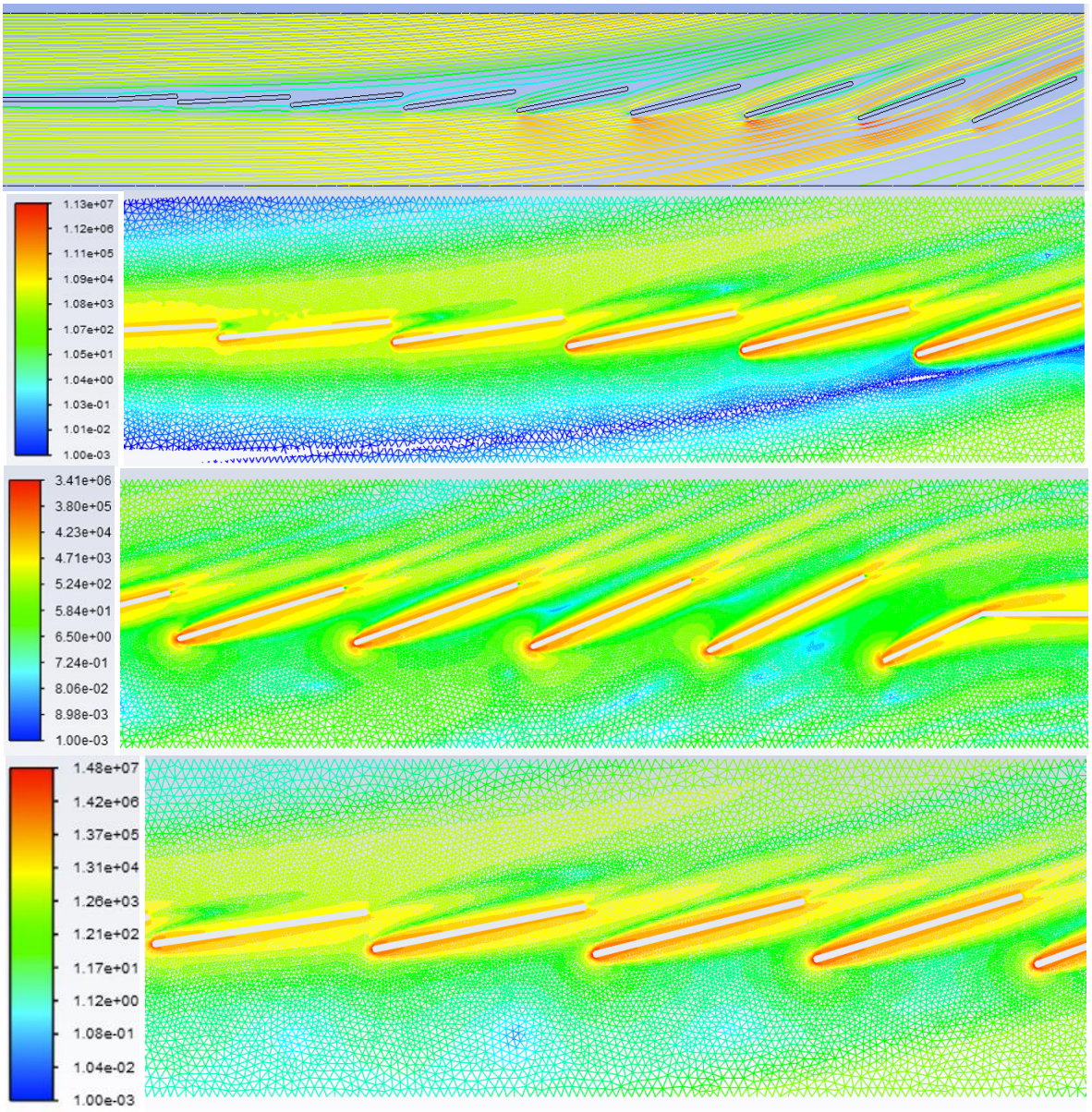

Figure 5: Variable attack angle. Top to bottom: streamlines, log-scale contours of $\dot{S}'''_{gen,T}$, $\dot{S}'''_{gen,V}$, and $\dot{S}'''_{gen,Total}$

4. CONCLUSIONS

Despite its confusing conception, we show that The Second Law of Thermodynamics is easy to use and interpret. We apply the numerical, local formulation to a simulation of a louvered fin heat exchanger using the common code package, Ansys Fluent. The user-defined functions are written separately for $\dot{S}'''_{gen,T}$ and $\dot{S}'''_{gen,V}$ using readily available temperature gradients and velocity gradients, respectively. The functions are then treated as field variables and then integrated and compared to determine where to focus the design effort.

Users of the First Law will say they can make the same design choices made in this paper without needing the Second Law. After all, the separate integrations of $\dot{S}'''_{gen,T}$ and $\dot{S}'''_{gen,V}$ are analogous to the total heat transfer rate and pumping power requirement, respectively. For experiments in which the only measurable quantities are the

temperatures and pressures surrounding the heat exchanger, First-Law users are just as effective as designers as Second-Law users. The argument in this paper becomes clear when designers begin to measure these quantities *inside* the heat exchanger with tools like particle image velocimetry or computational fluid dynamics.

Once a designer has access to detailed spatial measurements of temperature and velocity within the device, they can make more precise design changes. For example, a designer may recognize that large air-side velocity gradients generally imply a large fan power requirement. They could make design changes to reduce the velocity gradients in the same way as this paper with only a First-Law understanding. The problem is that these changes are often based on many years of 'best practice' using the First Law and that there is no fundamental way to quantify the objective locally within the device. The Second Law is the only way to quantify precisely when and where work is wasted.

NOMENCLATURE

C_p	specific heat	(J/kg-K)
F_d	air-side flow depth, or fin width	(mm)
F_l	fin length	(mm)
F_p	fin pitch	(mm)
f	Fanning friction factor	(–)
j	Colburn j-factor	(–)
k	turbulent kinetic energy	(m^2/s^2)
k_{cond}	thermal conductivity	(W/m-K)
L_l	louver length	(mm)
L_p	louver pitch	(mm)
P	pressure	(Pa)
q	heat flux	(W/m^2)
Re	Reynolds number	(–)
s	entropy	(J/kg-K)
$\dot{S}$	entropy generation	(W/K)
t	time	(second)
T	absolute temperature	(K)
T_p	tube pitch	(mm)
u	velocity	(m/s)
v	velocity	(m/s)
α	louver angle	(degrees)
δ_f	fin thickness	(mm)
ϵ	turbulent dissipation rate	(m^2/s^3)
μ	dynamic viscosity	(Pa-second)
Φ	viscous dissipation function	(s^{-2})
ρ	density	(kg/m^3)

Subscript

gen	generated
T	due to temperature gradients
Total	total i.e. T + V
V	due to velocity gradients
x	x-direction
y	y-direction

Superscript

$'''$	per unit volume

REFERENCES

ANSYS FLUENT 12.0 Theory Guide—4.4.3 Realizable—Model. (2009). Retrieved April 16, 2022, from https://www.afs.enea.it/project/neptunius/docs/fluent/html/th/node60.htm

Bejan, A. (1982). Second-Law Analysis in Heat Transfer and Thermal Design. In J. P. Hartnett & T. F. Irvine (Eds.), *Advances in Heat Transfer* (Vol. 15, pp. 1–58). Elsevier. https://doi.org/10.1016/S0065-2717(08)70172-2

Gouy. (1889). Sur l'énergie utilisable. *Journal de Physique Théorique et Appliquée*, *8*(1), 501–518. https://doi.org/10.1051/jphystap:018890080050101

Launder, B. E., & Spalding, D. B. (1974). The numerical computation of turbulent flows. *Computer Methods in Applied Mechanics and Engineering*, *3*(2), 269–289. https://doi.org/10.1016/0045-7825(74)90029-2

Park, Y.-G., & Jacobi, A. M. (2009). Air-Side Heat Transfer and Friction Correlations for Flat-Tube Louver-Fin Heat Exchangers. *Journal of Heat Transfer*, *131*(2), 021801. https://doi.org/10.1115/1.3000609

Shih, T.-H., Liou, W. W., Shabbir, A., Yang, Z., & Zhu, J. (1995). A new k-ϵ eddy viscosity model for high reynolds number turbulent flows. *Computers & Fluids*, *24*(3), 227–238. https://doi.org/10.1016/0045-7930(94)00032-T